galaxies

IMPACT FACTOR 2.5

CITESCORE 4.1

Article

# Quasiperiodic Oscillations and Dynamics of Test Particles around Regular-Kiselev Black Holes

Javlon Rayimbaev, Nozima Juraeva, Malika Khudoyberdiyeva, Ahmadjon Abdujabbarov and Mardon Abdullaev

MDPI

https://doi.org/10.3390/galaxies11060113

galaxies

MDPI

*Article*

# Quasiperiodic Oscillations and Dynamics of Test Particles around Regular-Kiselev Black Holes

**Javlon Rayimbaev [1,2,3,4,*], Nozima Juraeva [5,6], Malika Khudoyberdiyeva [4,5], Ahmadjon Abdujabbarov [5,7] and Mardon Abdullaev [8]**

[1] School of Mathematics and Natural Sciences, New Uzbekistan University, Mustaqillik Ave. 54, Tashkent 100007, Uzbekistan
[2] School of Engineering, Central Asian University, Tashkent 111221, Uzbekistan
[3] Institute of Fundamental and Applied Research, TIIAME National Research University, Kori Niyoziy 39, Tashkent 100000, Uzbekistan
[4] Faculty of Physics, National University of Uzbekistan, Tashkent 100174, Uzbekistan; xudoyberdiyeva94@inbox.ru
[5] Ulugh Beg Astronomical Institute, Astronomy Str. 33, Tashkent 100052, Uzbekistan; nozima@astrin.uz (N.J.); ahmadjon@astrin.uz (A.A.)
[6] Institute of Nuclear Physics, Ulugbek 1, Tashkent 100214, Uzbekistan
[7] Faculty of Computer Engineering, Tashkent University of Applied Sciences, Gavhar Str. 1, Tashkent 100149, Uzbekistan
[8] Power Engineering Faculty, Tashkent State Technical University, Tashkent 100095, Uzbekistan; mardon050592@gmail.com
* Correspondence: javlon@astrin.uz

**Abstract:** Testing gravity theories combining (massive and massless) scalar & electrodynamic fields become the most important issue in relativistic astrophysics using data from, black hole observations. In the present work, we first show a spherically symmetric black hole solution in general relativity coupling to generic-type nonlinear electrodynamics (NED) together with the quintessential field. We also obtain possible values for the parameters of the quintessential field and NED charge in the black hole environment for different values of degree of nonlinearity. Also, event horizon properties and scalar invariants of the black hole spacetime are studied. We investigate the equatorial motion of test particles around the regular-Kiselev black holes and study the combined effects of quintessential field and the NED charge of the black hole on particle angular momentum together with its energy at their circular orbits as well as their innermost circular stable orbits (ISCOs) and compared the obtained results with Reissner-Nordström black hole (RN BH) case. Moreover, we study particle oscillations along the orbits above than ISCO and applications to quasiperiodic oscillations (QPOs) where we obtain constrain values for the quintessential parameter and black hole mass charge parameters using observational QPO data from microquasars.

**Keywords:** black holes; nonlinear electrodynamics; quintessential field; quasiperiodic oscillations



**Citation:** Rayimbaev, J.; Juraeva, N.; Xudyoberdiyeva, M.; Abdujabbarov, A.; Abdullaev, M. Quasiperiodic Oscillations and Dynamics of Test Particles around Regular-Kiselev Black Holes. *Galaxies* **2023**, *11*, 113. https://doi.org/10.3390/galaxies11060113

Academic Editor: Peter Dunsby

Received: 11 September 2023
Revised: 22 October 2023
Accepted: 10 November 2023
Published: 16 November 2023



## 1. Introduction

In astrophysics, QPOs have been identified in the X-ray emissions of neutron stars and black holes, providing insights into the extreme gravitational environments near these objects. These quasiperiodic fluctuations in luminosity suggest the presence of underlying physical processes, such as oscillations of accretion disks or gravitational interactions, which could serve as probes to study the fundamental nature of spacetime.

The presence of QPOs in accretion disks around black holes suggests the existence of resonant oscillations that could be linked to the innermost stable circular orbits, shedding light on the strong gravity regime and testing Einstein's theory of general relativity. Neutron star QPOs, on the other hand, provide a platform to study the behavior of ultra-dense matter and the nuclear matter properties under extreme density and gravity conditions.

The interpretation of QPOs involves interdisciplinary collaboration, integrating theoretical models with observational data. Spectral-timing analysis and numerical simulations are employed to decipher the intricate interplay between accretion flows, magnetic fields, and gravitational interactions.

Furthermore, the observation of twin-peak QPOs in some systems has sparked debates about their origins and potential connections to oscillatory modes within the accretion disk. These findings underscore the need for advanced theoretical frameworks and more precise observational data. After the first detection of QPO in the analyses of the spectrum and the flux from X-ray binaries [1] have been studied in numerous works together with the theoretical investigations of QPO and their nature. The most promising model of QPO is related to particle dynamics and corresponding oscillations of their trajectories. From this point of view, QPOs resulting in the collective motion of test charged particles containing accretion disk have been investigated in [2–16].

Regular black holes, an intriguing concept in astrophysics, challenge the traditional notion of singularities at the center of astrophysical black holes. Unlike classical black holes that exhibit infinite curvature and density at their centers, regular black holes are proposed to possess a core where the spacetime curvature remains finite [17–23]. This idea has potential implications for resolving the information paradox and harmonizing quantum mechanics with general relativity [24–26].

Regular black holes are posited to be formed via mechanisms that prevent the complete collapse of matter, avoiding the formation of singularities. Various theoretical frameworks, such as modifications to Einstein's equations or the introduction of exotic forms of matter, have been proposed to describe these objects. One of the regularizations of black holes has been proposed within the Kiselev model [27].

Our aim of this work is to investigate test particle dynamics around regular Kiselev black holes and corresponding applications to describe QPOs. The paper is organized as follows: In Section 2 we review the generic regular black hole surrounded by a quintessential field. The Section 3 is devoted to studying the test particle dynamics around regular Kiselev black hole. We study the fundamental frequencies in spacetime around the regular Kiselev black hole in Section 4. In Section 5 we discuss the QPO models and possible applications to observed sources. We conclude our results in Section 7.

In this work, we use the geometrical system of units $G = c = 1$ and run the Greek indices from 0 to 3, and Latin indices from 1 to 3.

## 2. Generic Regular Black Holes in Quintessential Fields

The generic case of the regular back solution is obtained in Ref. [23], in general, relativity coupling to nonlinear electrodynamics with the following Lagrangian:

$$\mathcal{L}(F) = \frac{4\mu}{\alpha} \frac{(\alpha F)^{\frac{\nu+3}{4}}}{\left[1 + (\alpha F)^{\frac{\nu}{4}}\right]^{1+\frac{\mu}{\nu}}} \tag{1}$$

where dimensionless constants $\mu$ and $\nu$ are degree of nonlinearity, and can be $\mu > 3$ & $\nu > 0$, $\alpha$ dimension of length squared, and $F = \frac{1}{4} F_{\mu\nu} F^{\mu\nu}$, with $F_{\mu\nu} = 2\nabla_{[\mu} A_{\nu]}$, where $F_{\mu\nu}$ denotes the Maxwell electromagnetic field tensor.

However, we assume the generalized action for this theory as:

$$\mathcal{S} = \frac{1}{16\pi} \int d^4x \sqrt{-g}(R - \mathcal{L}(F) + \mathcal{L}_m), \tag{2}$$

where g is a determinant of the metric tensor, $R$ is the Ricci scalar curvature, and $\mathcal{L}_m$ is Lagrangian for an anisotropic matter field.

Here we consider the field as a quintessential field. The components of the non-vanishing stress-energy tensor of the field derived by Kiselev [27].

$$\begin{aligned} T_t^t &= T_r^r = \rho_q, \\ T_\theta^\theta &= T_\phi^\phi = -\frac{1}{2}\rho_q(1+3\omega_q), \end{aligned} \tag{3}$$

where $\omega_q$ is the state parameter of the corresponding equation of state of the quintessential field $p_q = \omega_q \rho_q$, and take values $-1 < \omega_q < -1/3$. When $\omega_q = 0$ corresponds to the Schwarzschild black hole case, $\omega_q = -1/3$ to RN BH case and the case $\omega_q = -1$ defines Schwarzschild-(anti)-de Sitter black hole spacetime. $\rho_q$ is the density which is always positive and $\rho_q = -3\omega_q(c/2)/r^{3(1+\omega_q)}$ and $c > 0$ is a normalization factor.

The GR BH spacetime satisfying the weak energy condition can be obtained by coupling Einstein's gravity to a nonlinear electrodynamic field [23,28]. This model is described by the metric given by

$$ds^2 = -f(r)dt^2 + \frac{1}{f(r)}dr^2 + r^2(d\theta^2 + \sin^2\theta d\phi^2), \tag{4}$$

with

$$f(r) = 1 - \frac{2M}{r}\left(1 + \frac{q^\nu}{r^\nu}\right)^{-\frac{\mu}{\nu}} - \frac{\mathcal{C}}{r^{3\omega_q+1}} \tag{5}$$

where $M$ is the total mass of the BH, and $q$ is the magnetic charge of a nonlinear self-gravitating monopole. When $q = \mathcal{C} = 0$ the solution (5) turns to the Schwarzschild solution, while at $\mathcal{C} = 0$, it becomes the generic regular black hole solution.

### 2.1. Horizon Structure

Here, we will analyze the radial profiles of the metric function $f(r)$.

In Figure 1, we analyze the zeros of the metric function (5) as a radial function by varying the non-linearity parameter $\nu$, the black hole charge $q$, and the quintessence field parameters $\mathcal{C}$, and $\omega_q$. Observed that when $\mathcal{C} = 0$ an increase of $\nu$ causes a decrease (increase) in the radius of the event (Cauchy) horizon. However, at $\omega_q = -1/2$, the radius of the event horizon increases with increasing $\nu$ and $\mathcal{C}$. When, $\nu$ changes from 0 to 1, the event horizon shifts out sufficiently, while in charges from 2 to 3, the horizon shift is very small.

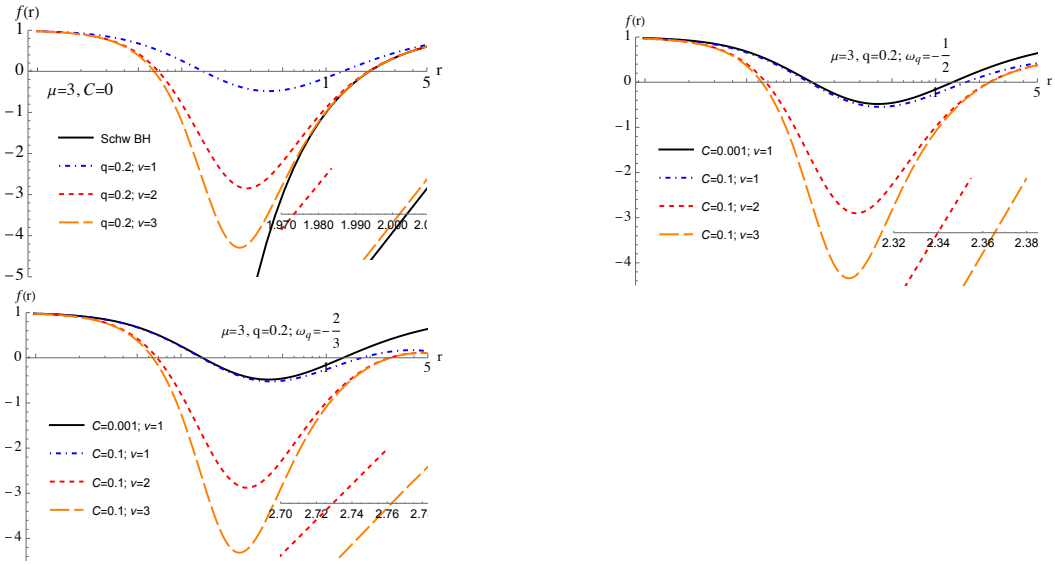


**Figure 1.** Radial profiles of $f(r)$ for different values of the black hole charge, nonlinearity, and quintessential field parameters. $M = 1$.

Now, we will find the separate are in values of the quintessence parameter $\mathcal{C}$ and the black hole charge $q$ which changes the event horizon oppositely, by two: black hole no black hole regions using the set of equations $f(r) = 0$ and $\partial_r f(r) = 0$. The black hole region means that when we choose the values for $q$ and $\mathcal{C}$ the metric (5) should have zeros, where black hole horizons exist. In the black hole region, the metric (5) determines the spacetime of horizonless objects, such as a naked singularity.

It is clearly observed from Figure 2 that with an increase of $\nu$ the maximum value of $\mathcal{C}$ decreases, however, extreme charge $q$ increases, and the black hole region expands.

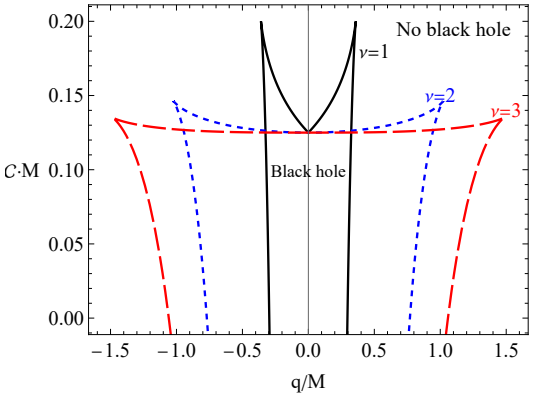


**Figure 2.** The relationships between the black hole magnetic charge ($q$) and the quintessential field parameter ($\mathcal{C}$) corresponding to a black hole. Black lines for $\nu = 1$, while the red dashed and blue large-dashed lines for $\nu = 2$, and $\nu = 3$ cases.

### *2.2. Scalar Invariants*

The curvature invariants of a spacetime are quantities that describe its curvature properties and are useful for understanding the geometry of spacetimes around black holes. Three well-known scalar curvature invariants are the Ricci scalar, the square of the Ricci tensor, and the Kretschmann scalar. By analyzing the behavior of the curvature invariants, we can learn about the geometry of spacetime. For example, the square of the Ricci tensor is defined as the square of the energy-momentum tensor of a field in the spacetime of a black hole as $\mathcal{R} = R_{\mu\nu}R^{\mu\nu} \equiv 1/(8\pi G)T_{\mu\nu}T^{\mu\nu}$. The Kretschmann scalar is responsible for the effective gravitational energy density of the spacetime ($\sqrt{\mathcal{K}} \sim \rho_M$). Now, we can calculate the Ricci scalar, the square of the Ricci tensor, and the Kretschmann scalar of spacetime (5). Due to the large form of their expressions, below, we plot to visualize the curvature properties of the spacetime and analyze them graphically.

Figure 3 shows the radial dependence of scalar invariants of spacetime (5), such as the Ricci scalar in the top left panel, the square of the Ricci tensor in the top right panel, and the Kretchman scalar (square of Riemann tensor) in the bottom panel. One can see from the figure that an increase in the values of $\nu$ and $\mathcal{C}$ causes an increase in the Ricci scalar and square of the Ricci tensor, while the Kretchman scalar decreases.

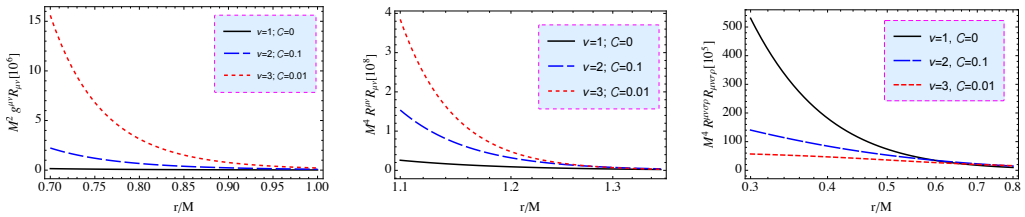


**Figure 3.** Radial profiles of scalar invariants.

## 3. Test Particles in the Spacetime of the Regular-Kiselev Black Holes

In the present section, we consider the effects of NED and quintessential fields on particle dynamics around spherically symmetric black holes.

### 3.1. Deriving Equations of Electrically Particles Motion

The equations of motion for massive electrically neutral particles govern using time-like geodesics of the spacetime (5).

Taking into account integrals of motion, such as the particle's specific energy $\mathcal{E} = E/m$ and its angular momentum $\mathcal{L} = L/m$, one may derive the equations in the form,

$$\dot{r}^2 = \mathcal{E}^2 + g_{tt}\left(1 + \frac{\mathcal{K}}{r^2}\right), \tag{6}$$

$$\dot{\theta} = \frac{1}{g_{\theta\theta}^2}\left(\mathcal{K} - \frac{l^2}{\sin^2\theta}\right), \tag{7}$$

$$\dot{\phi} = \frac{l}{g_{\phi\phi}}, \tag{8}$$

$$\dot{t} = -\frac{\mathcal{E}}{g_{tt}}, \tag{9}$$

where $\mathcal{K}$ is the Carter constant which corresponds to the particle's angular momentum.

Furthermore, one may restrict the dynamics of the particles to some constant plane as $\theta = \theta_0 =$ const and that implies the momentum along $\theta$ is zero ($\dot{\theta} = 0$). Consequently, the Carter constant takes $\mathcal{K} = \mathcal{L}^2/\sin^2\theta_0$. Thus, the equation of motion in the constant plane takes in the following form

$$\dot{r}^2 = \mathcal{E}^2 - V_{\text{eff}}(r), \tag{10}$$

where $V_{\text{eff}}(r)$ is the effective potential corresponding to circular motion which has with the form,

$$V_{\text{eff}}(r) = f(r)\left(1 + \frac{\mathcal{L}^2}{r^2\sin^2\theta_0}\right). \tag{11}$$

In order to observe the effects of the charge ($q$) sourced by the NED field and the quintessential field on the effective potential at the equatorial plane, we analyze it graphically for different values of the quintessential field and nonlinearity parameters in Figure 4.

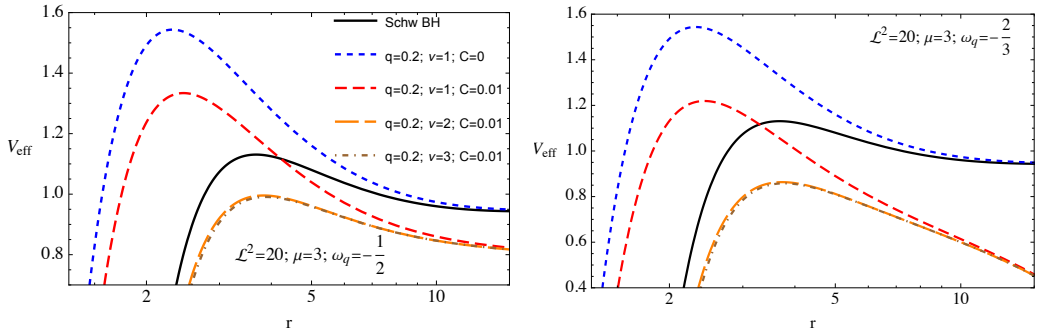


**Figure 4.** The effective potential as a function of the radial coordinate for different $q, \nu, \mathcal{C}$ and $\omega_q$ parameters. $M = 1$.

It is observed from Figure 4 that the presence of NED charge causes an increase in the maximum of the effective potential and the orbit where the effective potential takes maximum shifts towards the black hole. While the maximum decrease is due to the presence of the quintessential field. Also, the effective potential at larger distances decreases at smaller values of the $\omega_q$ parameter.

### 3.2. Circular Orbits

The circularity of the orbits of test particles orbiting a central black hole is described by the following conditions.

$$V_{\text{eff}} = \mathcal{E}, \qquad V'_{\text{eff}} = 0\,. \tag{12}$$

In circular orbits, no radial motion means that radial forces compensate each other at the corresponding values of angular momentum of the particles. Expressions of the particle energy and its angular momentum along circular orbits in the equatorial plane using the conditions (12) in the form

$$\mathcal{L}^2 = \frac{r^3\left(2Mr(2q^\nu - r^\nu) + \mathcal{C}(q^\nu + r^\nu)^{\frac{\nu+3}{\nu}}\right)}{6Mr^{\nu+2} + (\mathcal{C}r - 2)(q^\nu + r^\nu)^{\frac{\nu+3}{\nu}}}, \tag{13}$$

$$\mathcal{E}^2 = -\frac{2(q^\nu + r^\nu)^{\frac{\nu-3}{\nu}}\left[2Mr^2 + (\mathcal{C}r - 1)(q^\nu + r^\nu)^{\frac{3}{\nu}}\right]^2}{6Mr^{\nu+2} + (\mathcal{C}r - 2)(q^\nu + r^\nu)^{\frac{\nu+3}{\nu}}}. \tag{14}$$

Figure 5 presents radial profiles of specific energy and angular momentum of the particles for fixed values of the parameters $\mu = 3$, $C = 0.25$ and $\omega_q = -1/3$ and different values of the parameter $\nu$. Moreover, to show the effects of the quintessential medium and the feature of the nonlinear electrodynamics, in the figures, we have also provided the plots for the energy and angular momentum of test particles around RN BH. It is shown that the existence of the quintessential medium with the parameter $\omega_q = -1/3$ decreases the asymptotics of the energy values. Vice versa, an increase in $\nu$ also causes to increase in it. However, the effect of the NED field is more sensitive to the angular momentum compared to the energy and causes an increase over that of the RN BH case.

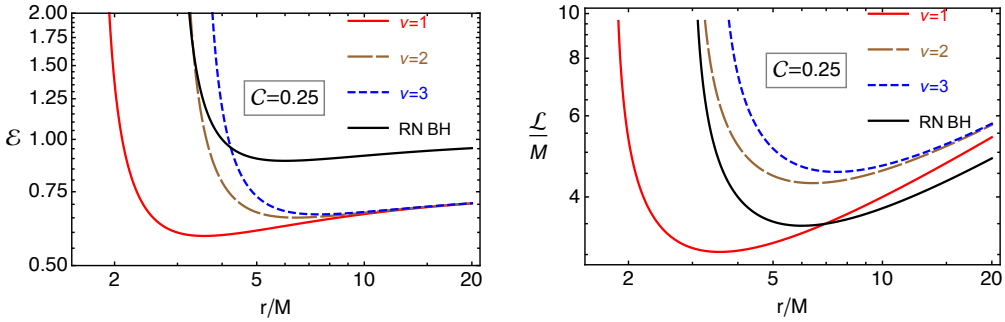


**Figure 5.** Specific energy and angular momentum of test particles corresponding to circular orbits around regular generic BH in the quintessential field. In this graph, we have fixed values for the parameters $\mu = 3$, $C = 0.25$, and $\omega_q = -1/3$ as shown in this graph, by varying the parameter $\nu = 1, 2, 3$ with the comparison of the results obtained in RN BH.

### *3.3. ISCO Studies*

The ISCO is an important concept in the study of black holes and accretion disks around them, and it is a region of spacetime where the gravitational field of the black hole is extremely strong and also where the physics of accretion disks is most complex. The material in the accretion disk will eventually spiral inwards and cross the ISCO. Once particles cross the ISCO, they will inevitably fall into the central black hole. In fact, the circular orbits can be stable when the effective potential satisfies the condition $\partial_{rr} V_{\rm eff}(r_{\rm ISCO}) > 0$, while ISCO satisfies $\partial_{rr} V_{\rm eff}(r_{\rm ISCO}) = 0$, mostly, together with the conditions (12). One may get the following equation using the ISCO conditions,

$$2\mathcal{C}(3 - \mathcal{C}r)(q^\nu + r^\nu)^{\frac{6}{\nu}+2} + 24M^2 r^{\nu+3}((\nu - 2)q^\nu + r^\nu) - 4Mr(q^\nu + r^\nu)^{\frac{2}{\nu}} \times \left[q^{2\nu}(3\mathcal{C}r - 8) + q^\nu r^\nu(3\nu - 3\mathcal{C}\nu r + 2) + (6\mathcal{C}r + 1)r^{2\nu}\right] = 0\,. \tag{15}$$

Equation (15) is impossible to solve concerning $r$, thus we obtain contour plots of the equation for different NED fields and quintessential field parameters.

In Figure 6, the dependence of ISCO of a neutral particle orbiting regular generic BH in the quintessential field on the fixed values of parameters $\mu = 3$, $C = 0.01$ and $\omega_q = -2/3$

and different values of $\nu$ parameter. The value of $\nu$ increases (decreases), and the minimum value of the radius of ISCO also increases (decreases).

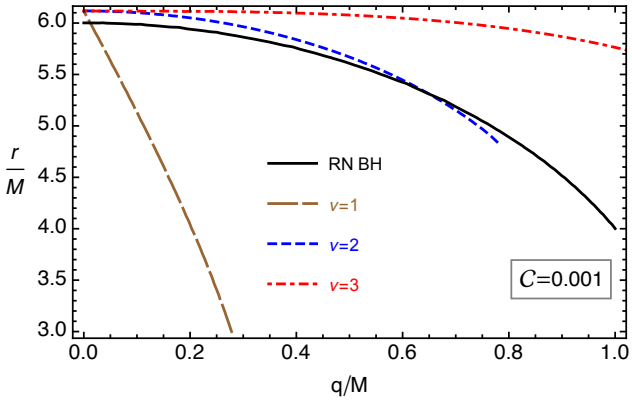


**Figure 6.** The ISCO radius as a function of the charge for the different values of the parameter $\nu$.

We have obtained that the ISCO radius decreases faster as $\nu = 1$ compared with $\nu = 2, 3$ cases as well as the case of magnetically Reissner-Nordström black hole case. That means in the $\nu = 1$ case, the gravitational effect of the charge $q$ is much stronger than in the other cases.

## 4. Fundamental Frequencies

Here we consider the fundamental frequencies in oscillations of test particles orbiting a regular black hole in the quintessential field. In particular, the orbital frequencies of the particles in their Keplerian orbits and the radial and vertical oscillation frequencies along the orbits are higher than ISCOs, and we apply them to QPO analyses.

### *4.1. Keplerian Frequency*

The angular velocity of the particles in circular orbits $\Omega_K = \dot{\phi}/\dot{t}$ around regular-Kiselev black holes take th form,

$$\Omega_K^2 = \frac{M(r^\nu - 2q^\nu)}{(q^\nu + r^\nu)^{\frac{\nu+3}{\nu}}} - \frac{\mathcal{C}}{2r}.$$

Furthermore, we express all the frequencies in the unit of Hz, multiplying by $c/(2\pi GM)\Omega$. We take the speed of light as $c = 3 \times 10^8$ m/sec, and the gravitational Newtonian constant as $G = 6.67 \times 10^{-11}$ m$^3$/(kg$^2$ $\times$ sec).

### *4.2. The Radial and Vertical Oscillation Frequencies*

The test particles orbiting a black hole along stable circular orbits may oscillate in the directions of the radial and vertical axes, due to small displacement $r_0 + \delta r$ and $\pi/2 + \delta\theta$. Harmonic oscillator equations The frequencies of radial and vertical oscillations can be evaluated by the following [29]:

$$\frac{d^2\delta r}{dt^2} + \Omega_r^2 \delta r = 0\,, \qquad \frac{d^2\delta\theta}{dt^2} + \Omega_\theta^2 \delta\theta = 0\,, \tag{16}$$

where

$$\Omega_r^2 = -\frac{1}{2g_{rr}(u^t)^2}\partial_r^2 V_{\rm eff}(r,\theta)\Big|_{\theta=\pi/2}\,, \tag{17}$$

$$\Omega_\theta^2 = -\frac{1}{2g_{\theta\theta}(u^t)^2}\partial_\theta^2 V_{\rm eff}(r,\theta)\Big|_{\theta=\pi/2}\,, \tag{18}$$

are the frequencies of radial and vertical oscillations, respectively.

## 5. QPO Models

In this section, we theoretically apply the fundamental frequencies to obtain high-frequency upper and lower frequencies ($\nu_U$ and $\nu_L$) in twin QPOs. Several QPO models explain the QPO frequencies as combinations of Keplerian, radial, and vertical frequencies of test particles, i.e., the peak frequencies are described in terms of frequencies of radial and vertical oscillations and Keplerian frequency. For example, according to the RP model, $\nu_U$ is interpreted as orbital frequency ($\nu_U = \nu_\phi$) while the lower frequency is the difference between Keplerian and radial frequencies in stable orbits $\nu_L = \nu_\phi - \nu_r$. Now, we analyze relationships between $\nu_U$ and $\nu_L$ to QPOs generated around regular black holes surrounded by quintessential fields by test particles.

In Figure 7 we demonstrate the relations between the upper and lower frequencies of the twin-peaked QPOs generated around the generic regular BH for various values of the nonlinearity parameter $\nu$, and the quintessential field parameter. Here, the black hole mass is chosen as 10 $M_\odot$, the NED field parameter $\mu = 3$. In the top left panel, we present the effects of the NED charge of the black hole and nonlinearity parameters on the upper and lower frequencies in the absence of the quintessential field. The frequency ratio at $\nu = 1$ is observed to be more significant than in the case $\nu = 2$ in the range of $\nu_U < 200$ Hz. Furthermore, low-frequency QPOs below 20 Hz disappear in the presence of a quintessential field with $\mathcal{C} = 0.001$, and the variation of $\omega_q$ does not give much change in QPO frequencies.

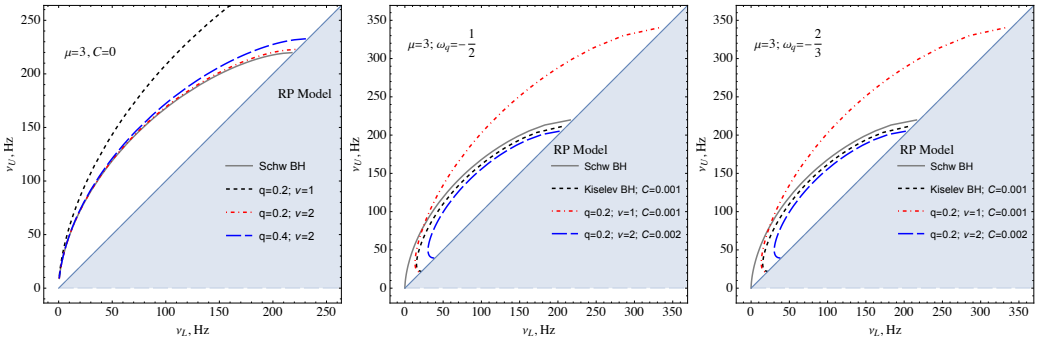


**Figure 7.** The figure shows the $\nu_U - \nu_L$ diagram for twin peak QPOs in the RP model (the top left panel for $\mathcal{C} = 0$ case, the top right one for $\mathcal{C} = 0.001$ & $\omega_q = -\frac{1}{2}$ and the bottom one for $\omega_q = -\frac{2}{3}$ case).

*QPO Orbits*

For the first time, R. Sunyaev has suggested that rotating and nonrotating black holes can be distinguished by signals generated by oscillated particles in orbits close to ISCO, called QPOs. According to his idea, one may measure ISCOs around black holes by studying QPO orbits. Our previous papers [my papers] showed that twin-peak QPOs are generated in stable orbits close to the ISCO in the framework of various gravity theories. As the frequency ratio tends to 1, the QPO orbit approaches ISCO. In this subsection, we consider the radius of QPO orbits around regular black holes in the quintessential field in the RP. One may obtain the dependence of the QPO radius from the black hole charge by solving the equation with respect to $r$,

$$3\nu_L(r; q, \nu, \mu, \mathcal{C}, \omega_q) = 2\nu_U(r; q, \nu, \mu, \mathcal{C}, \omega_q), \tag{19}$$

Now we are interested in how the QPO orbits depend on the black hole, NED, and quintessential field parameters. Figure 8 shows the dependence of the radius of QPO orbits for different values of nonlinearity and quintessential field parameters. Our performed analyses have shown that an increase in the black hole charge causes a decrease in the radius. It decreases faster at $\nu = 1$ case compared to $\nu = 2, 3$ cases which means the gravitational effect of the black hole charge becomes weaker at higher values of the nonlinearity parameter $\nu$ weak. However, the orbit shifts slightly out due to the presence

of a quintessential field. Also, an increase of the $\omega_q$ parameter slightly increases the radius (see Figure 9).

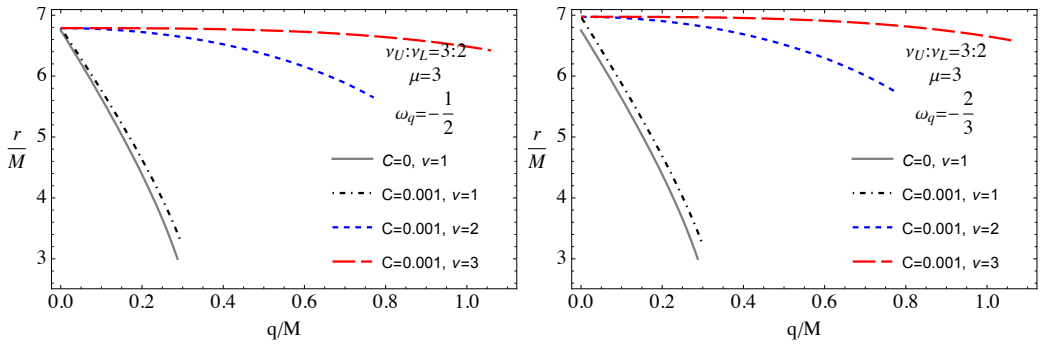


**Figure 8.** Dependence of the radius of the orbits where QPOs occur with the frequency ratio 3:2 from the magnetic charge $q$ for various values of $\nu$ and $\mathcal{C}$. Left panel for $\omega_q = -\frac{1}{2}$ and right one for $\omega_q = -\frac{2}{3}$. Analyses are done in the RP model.

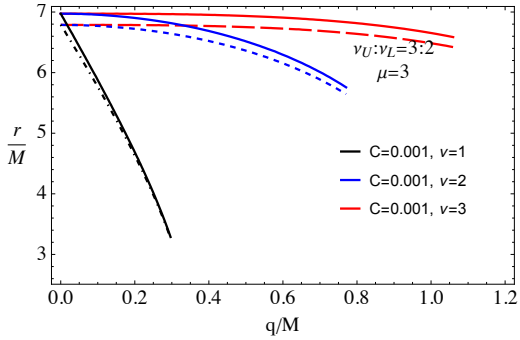


**Figure 9.** The same figure with Figure 8 but for fixed values of $\mathcal{C} = 0.001$. Solid lined for $\omega_q = -\frac{2}{3}$ and dashed ones for $\omega_q = -\frac{1}{2}$.

## 6. Constraining Black Hole Mass and Its Magnetic Charge Using QPO Data

The $\chi^2$ method is a powerful tool for constraining the parameters of black hole models. It has been used to constrain the parameters of black holes in gravity theories in a variety of astrophysical systems, including active galactic nuclei, (low-mass) X-ray binaries, and gravitational wave sources. Here we obtain the constraints for mass and charge of the regular black hole in a quintessential field using QPOs data observed in the microquasars GRS 1915+105 and GRO J1655-40 performing $\chi^2$-method analyses [30]

$$\begin{aligned}\chi^2(M,B,r_1,r_2) &= \frac{(\nu_{1\phi}-\nu_{1\mathrm{U}})^2}{\sigma_{1\mathrm{U}}^2}+\frac{(\nu_{1\mathrm{per}}-\nu_{1\mathrm{L}})^2}{\sigma_{1\mathrm{L}}^2}\\ &+ \frac{(\nu_{1\mathrm{nod}}-\nu_{1\mathrm{C}})^2}{\sigma_{1\mathrm{C}}^2}+\frac{(\nu_{2\phi}-\nu_{2\mathrm{U}})^2}{\sigma_{2\mathrm{U}}^2}+\frac{(\nu_{2\mathrm{nod}}-\nu_{2\mathrm{C}})^2}{\sigma_{2\mathrm{C}}^2}\,. \end{aligned} \quad (20)$$

### *6.1. QPOs from GRO J1655-40*

The microquasar GRO J1655-40 is a black hole candidate binary system located in the constellation Scorpius. It is one of the most well-studied black hole candidates, and it has been used to constrain the parameters of black holes and to test theories of gravity. This subsection is devoted to obtaining constraint values of the black hole mass and its NED charge surrounding a quintessential field using observed QPO frequencies in the microquasar GRO J1655-40 [11],

$$\begin{aligned} \nu_{1U} &= 441 \text{ Hz}, & \sigma_{1U} &= 2 \text{ Hz}, \\ \nu_{1L} &= 298 \text{ Hz}, & \sigma_{1L} &= 4 \text{ Hz}, \\ \nu_{1C} &= 17.3 \text{ Hz}, & \sigma_{1C} &= 0.1 \text{ Hz}, \end{aligned} \tag{21}$$

and

$$\begin{aligned} \nu_{2U} &= 451 \text{ Hz}, & \sigma_{2U} &= 5 \text{ Hz}, \\ \nu_{2C} &= 18.3 \text{ Hz}, & \sigma_{2C} &= 0.1 \text{ Hz}. \end{aligned} \tag{22}$$

Our $\chi^2$-analyses have shown that the error reaches its minimum at $r \simeq 4.60986\ M$, $q \simeq -0.9695\ M_\odot$, $M \simeq 6.60771\ M_\odot$, and $\mathcal{C} = 0.00199784/\sqrt{M}$ when $\omega_q = -\frac{2}{3}$ and equals to $\chi^2_{min} = 2.35409 \times 10^{-11}$. While for the case $\omega_q = -\frac{1}{2}$, $\chi^2_{min} = 5.99518 \times 10^{-11}$, at $r \simeq 4.68708\ M$, $q \simeq 0.481337\ M_\odot$, $M \simeq 3.21581\ M_\odot$ and $\mathcal{C} = 0.297692/M$.

### *6.2. QPOs from GRS 1915+105*

The QPOs in GRS 1915+105 have also been used to test theories of gravity. For example, the frequency of the type-C QPO has been used to constrain the mass and spin of the black hole in GRS 1915+105. This information has been used to test different models of black holes, such as the Kerr metric. Here, we get black hole mass and charge constraints by performing similar analyses done in the above subsection, but for QPO data from the GRS 1915+105 microquasar [31],

$$\begin{aligned} \nu_{1U} &= 184.10 \text{ Hz}, & \sigma_{1U} &= 1.84 \text{ Hz}, \\ \nu_{2U} &= 142.98 \text{ Hz}, & \sigma_{2U} &= 3.48 \text{ Hz}, \end{aligned} \tag{23}$$

and

$$\begin{aligned} \nu_{1L} &= 67.40 \text{ Hz}, & \sigma_{1L} &= 0.60 \text{ Hz}, \\ \nu_{2L} &= 65.89 \text{ Hz}, & \sigma_{2L} &= 0.52 \text{ Hz}, \\ \nu_{3L} &= 69.58 \text{ Hz}, & \sigma_{3L} &= 0.49 \text{ Hz}. \end{aligned} \tag{24}$$

Here, we also perform similar numerical analyses for the cases $\omega_q = -\frac{2}{3}$ and $\omega_q = -\frac{1}{2}$. It is obtained that in the case $\omega_q = -\frac{2}{3}$, the minimum of $\chi^2_{min} = 3.8563 \times 10^{-11}$ at the values of the QPO orbit $r \simeq 10.5034\ M$, the black hole charge $q \simeq 0.518973\ M_\odot$, quintessential field parameter $\mathcal{C} \to 0.00357793/\sqrt{M}$, and the black hole mass $M \to 5.02719\ M_\odot$.

And when $\omega_q = -\frac{1}{2}$, the minimum is about $\chi^2_{min} = 4.7845 \times 10^{-10}$, at $r \simeq 13.9982\ M$, $q \simeq -1.18079\ M_\odot$, $\mathcal{C} \simeq 0.0237965/M$, and $M \simeq 2.97625\ M_\odot$.

In Figures 10 and 11 we have shown constraint values for the electric charge and mass of the black hole located at the microquasars GRO J1655-40 and GRS 1915-105, respectively, for different nonlinearity and quintessential field parameters in the $1\sigma$, $2\sigma$, and $3\sigma$ error bars.

### *6.3. Comparisons of the Black Hole Mass Constraints with Other Independent Findings*

Here, in order to compare our results, we provide black hole mass constraints in the above-mentioned microquasars obtained using independent observations such as the X-ray timing techniques; their estimations on the mass of the central black hole in the microquasar GRO J1655-40 has mass $M/M_\odot = 5.31 \pm 0.07$ [32].

The constraints on the black hole mass using QPOs data considering the central black hole as a rotating Kerr black hole in the RP model have been obtained as $M/M_\odot = 5.3 \pm 0.1$ in Ref. [33].

Constraints of the black hole mass in the microquasar GRS 1915+105 obtained using the infrared spectroscopy technique as $M/M_\odot = 12 \pm 1.4$ [34], using QPOs data and considering the black hole as a Kerr black hole as $M/M_\odot = 13.1 \pm 0.2$ [35].

In fact, constraints on black hole parameters using astrophysical observations strongly depend on the type of observation data, its accuracy, and the gravity model of the black

hole spacetime, as well as the theoretical model of the study. Therefore, obtained constraint values may differ from each other for different black holes in different observational data. Unfortunately, it is quite hard to know which one is more trustworthy. It is seen from the above-mentioned constraints from independent measurement that our results differ from them. In our theoretical model, the test particles feel combined gravitational effects of the black hole mass, NED field, and quintessential field on the spacetime around black holes. Consequently, our obtained results show not only constraints on the black hole mass and charge but also the value of the quintessential parameter for the models of the equation of state of the quintessential field $\omega_q = -1/2$ and $\omega_q = -2/3$.

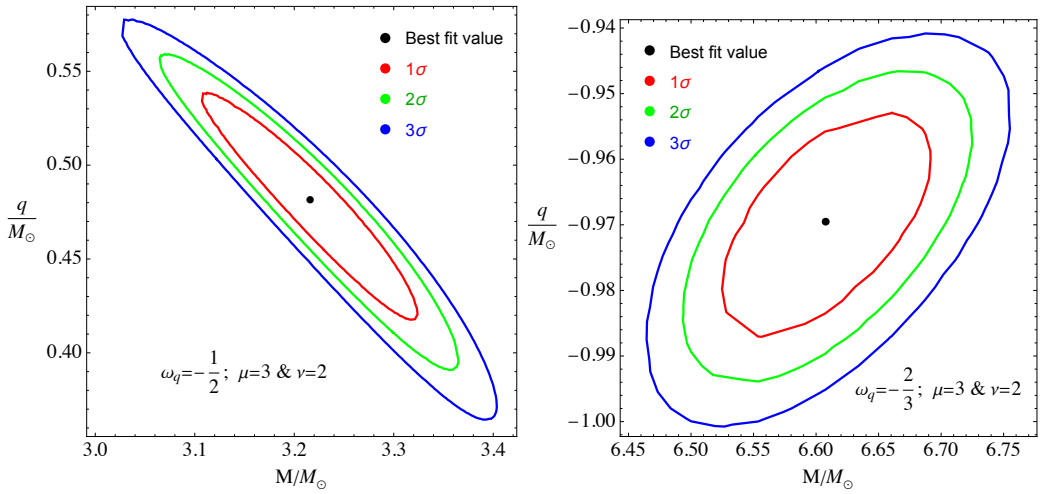


**Figure 10.** Constraints on the mass and charge of the black hole located at the center of the microquasar GRO J1655-40 in the presence of quintessential and NED fields.

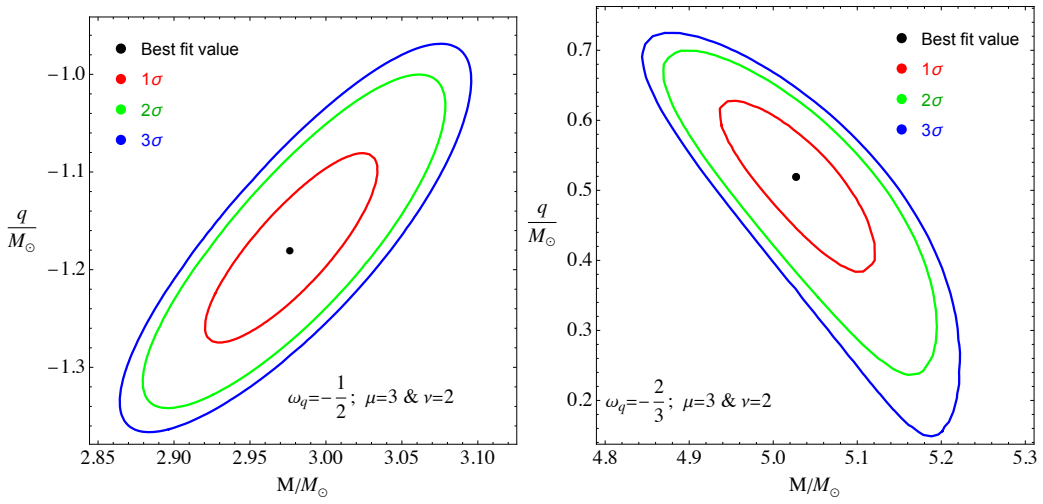


**Figure 11.** Similar plots Figure 10, but for GRS 1915-105.

## 7. Conclusions

In fact, testing gravity theories combined with different including massive and massless scalar and linear/nonlinear electrodynamics fields using observational data from black holes and neutron stars is the most important and actual issue in modern relativistic astrophysics. In this paper, we have obtained a new spherically symmetric black hole solution in general relativity coupling to nonlinear electrodynamics (NED) and quintessential fields. Also, we have analyzed the possible values for the quintessential field parameter and NED charge of the black hole for various values of the nonlinearity parameter $\nu$ in the $\omega_q = -\frac{2}{3}$ case. Event horizon properties and scalar invariants of the black hole spacetime are studied. We have investigated the motion of test particles around the regular Kiselev black

holes in the equatorial plane and studied the combined effects of the quintessential field and the NED charge of the black hole on the angular momentum and energy of particles corresponding to circular orbits together with their ISCOs. Moreover, we calculated the oscillation frequencies of the particles along stable circular orbits in radial and vertical directions together with the Keplerian frequency. Then, we applied the frequencies to study QPOs in the RP model. It is shown that low-frequency QPOs below 20 Hz disappear in the presence of quintessential field with $\mathcal{C} = 0.001$, and the variation of $\omega_q$ does not give much change in QPO frequencies. Also, we have obtained the dependence of the radius of orbits where the QPOs with the frequency ratio is 3:2, on the black hole charge for different nonlinearity and quintessential field parameters. Our performed analyses have shown that an increase in the black hole charge causes a decrease in the radius. It decreases faster at $\nu = 1$ case compared to $\nu = 2, 3$ cases which means the gravitational effect of the black hole charge becomes weaker at higher values of the nonlinearity parameter $\nu$ weak. However, the orbit shifts slightly out due to the presence of a quintessential field. Also, an increase of the $\omega_q$ parameter slightly increases the radius.

Finally, we have obtained constrain values for the quintessential parameter together with the black hole mass and its charge using observational data from QPOs observed in the microquasars GRO J1655-40 and GRS 1915+105 performing $\chi^2$-method analyses and compared the obtained results with the mass constraints obtained in the independent astronomical observations.

**Author Contributions:** Conceptualization, J.R. and A.A.; methodology, J.R.; software, J.R. and M.A.; validation, N.J. and M.K.; formal analysis, J.R. and A.A.; investigation, A.A. and J.R. All authors have read and agreed to the published version of the manuscript.

**Funding:** Grants of the Ministry of Higher Education, Science, and Innovation of the Republic of Uzbekistan: F-FA-2021-432, F-FA-2021-510, and MRB-2021-527.

**Institutional Review Board Statement:** Not applicable.

**Informed Consent Statement:** Not applicable.

**Data Availability Statement:** Data are contained within the article.

**Acknowledgments:** A.A. and J.R. acknowledge Grants of the Ministry of Higher Education, Science, and Innovation of the Republic of Uzbekistan.

**Conflicts of Interest:** The authors declare no conflict of interest.

## References

1. Angelini, L.; Stella, L.; Parmar, A.N. The Discovery of 0.2 HZ Quasi-periodic Oscillations in the X-ray Flux of the Transient 42 Second Pulsar EXO 2030+374. *Astrophys. J.* **1989**, *346*, 906. [CrossRef]
2. Kato, S.; Fukue, J. Trapped Radial Oscillations of Gaseous Disks around a Black Hole. *Publ. Astron. Soc. Jpn.* **1980**, *32*, 377. [CrossRef]
3. Abramowicz, M.A.; Kluźniak, W. A precise determination of black hole spin in GRO J1655-40. *Astron. Astrophys.* **2001**, *374*, L19–L20. [CrossRef]
4. Wagoner, R.V.; Silbergleit, A.S.; Ortega-Rodríguez, M. "Stable" Quasi-periodic Oscillations and Black Hole Properties from Diskoseismology. *Astrophys. J. Lett.* **2001**, *559*, L25–L28. [CrossRef]
5. Silbergleit, A.S.; Wagoner, R.V.; Ortega-Rodríguez, M. Relativistic Diskoseismology. II. Analytical Results for C-modes. *Astrophys. J.* **2001**, *548*, 335–347. [CrossRef]
6. Wang, D.H.; Chen, L.; Zhang, C.M.; Lei, Y.J.; Qu, J.L.; Song, L.M. Investigation of the emission radii of kHz QPOs for the accreting millisecond X-Ray pulsars, Atoll and Z sources. *Mon. Not. R. Astron. Soc.* **2015**, *454*, 1231–1237. [CrossRef]
7. Rezzolla, L.; Yoshida, S.; Maccarone, T.J.; Zanotti, O. A new simple model for high-frequency quasi-periodic oscillations in black hole candidates. *Mon. Not. R. Astron. Soc.* **2003**, *344*, L37–L41. [CrossRef]
8. Török, G.; Stuchlík, Z. Radial and vertical epicyclic frequencies of Keplerian motion in the field of Kerr naked singularities. Comparison with the black hole case and possible instability of naked-singularity accretion discs. *Astron. Astrophys.* **2005**, *437*, 775–788. [CrossRef]
9. Ingram, A.; Done, C. A physical interpretation of the variability power spectral components in accreting neutron stars. *Mon. Not. R. Astron. Soc.* **2010**, *405*, 2447–2452. [CrossRef]

10. Fragile, P.C.; Straub, O.; Blaes, O. High-frequency and type-C QPOs from oscillating, precessing hot, thick flow. *Mon. Not. R. Astron. Soc.* **2016**, *461*, 1356–1362. [CrossRef]
11. Stuchlík, Z.; Kotrlová, A.; Török, G. Multi-resonance orbital model of high-frequency quasi-periodic oscillations: Possible high-precision determination of black hole and neutron star spin. *Astron. Astrophys.* **2013**, *552*, A10. [CrossRef]
12. Stuchlík, Z.; Kotrlová, A.; Török, G. Resonant Switch Model of Twin Peak HF QPOs Applied to the Source 4U 1636-53. *Acta Astron.* **2012**, *62*, 389–407. [CrossRef]
13. Ortega-Rodríguez, M.; Solís-Sánchez, H.; Álvarez-García, L.; Dodero-Rojas, E. On twin peak quasi-periodic oscillations resulting from the interaction between discoseismic modes and turbulence in accretion discs around black holes. *Mon. Not. R. Astron. Soc.* **2020**, *492*, 1755–1760. [CrossRef]
14. Stuchlík, Z.; Kološ, M.; Kovář, J.; Slaný, P.; Tursunov, A. Influence of Cosmic Repulsion and Magnetic Fields on Accretion Disks Rotating around Kerr Black Holes. *Universe* **2020**, *6*, 26. [CrossRef]
15. Maselli, A.; Pappas, G.; Pani, P.; Gualtieri, L.; Motta, S.; Ferrari, V.; Stella, L. A New Method to Constrain Neutron Star Structure from Quasi-periodic Oscillations. *Astrophys. J.* **2020**, *899*, 139. [CrossRef]
16. Rayimbaev, J.; Dialektopoulos, K.F.; Sarikulov, F.; Abdujabbarov, A. Quasiperiodic oscillations around hairy black holes in Horndeski gravity. *Eur. Phys. J. C* **2023**, *83*, 572. [CrossRef]
17. Bardeen, J. *Proceedings of the GR5*; DeWitt, C., DeWitt, B., Eds.; Gordon and Breach: Tbilisi, Georgia, 1968; p. 174.
18. Ayón-Beato, E.; García, A. Regular Black Hole in General Relativity Coupled to Nonlinear Electrodynamics. *Phys. Rev. Lett.* **1998**, *80*, 5056–5059. [CrossRef]
19. Ayon-Beato, E. New regular black hole solution from nonlinear electrodynamics. *Phys. Lett. B* **1999**, *464*, 25–29. [CrossRef]
20. Toshmatov, B.; Abdujabbarov, A.; Ahmedov, B.; Stuchlík, Z. Particle motion and Penrose processes around rotating regular black hole. *Astrophys. Space Sci.* **2015**, *357*, 41. [CrossRef]
21. Toshmatov, B.; Ahmedov, B.; Abdujabbarov, A.; Stuchlík, Z. Rotating regular black hole solution. *Phys. Rev. D* **2014**, *89*, 104017. [CrossRef]
22. Övgün, A.; Sakallı, I.; Saavedra, J.; Leiva, C. Shadow cast of noncommutative black holes in Rastall gravity. *Mod. Phys. Lett. A* **2020**, *35*, 2050163. [CrossRef]
23. Toshmatov, B.; Stuchlík, Z.; Ahmedov, B. Comment on "Construction of regular black holes in general relativity". *Phys. Rev. D* **2018**, *98*, 028501. [CrossRef]
24. Turimov, B. On generic rotating regular black hole solutions. *Ann. Phys.* **2021**, *434*, 168658. [CrossRef]
25. Toshmatov, B.; Stuchlík, Z.; Ahmedov, B. Electromagnetic perturbations of black holes in general relativity coupled to nonlinear electrodynamics: Polar perturbations. *Phys. Rev. D* **2018**, *98*, 085021. [CrossRef]
26. Toshmatov, B.; Stuchlík, Z.; Schee, J.; Ahmedov, B. Electromagnetic perturbations of black holes in general relativity coupled to nonlinear electrodynamics. *Phys. Rev. D* **2018**, *97*, 084058. [CrossRef]
27. Kiselev, V.V. Quintessence and black holes. *Class. Quant. Gravity* **2003**, *20*, 1187–1197. [CrossRef]
28. Fan, Z.Y.; Wang, X. Construction of regular black holes in general relativity. *Phys. Rev. D* **2016**, *94*, 124027. [CrossRef]
29. Turimov, B.; Rahimov, O. The Orbital and Epicyclic Frequencies in Axially Symmetric and Stationary Spacetime. *Universe* **2022**, *8*, 507. [CrossRef]
30. Bambi, C. Testing the nature of the black hole candidate in GRO J1655-40 with the relativistic precession model. *arXiv* **2013**, arXiv:1312.2228. [CrossRef]
31. Belloni, T.; Soleri, P.; Casella, P.; Méndez, M.; Migliari, S. High-frequency quasi-periodic oscillations from GRS 1915+105 in its C state. *Mon. Not. R. Astron. Soc.* **2006**, *369*, 305–310. [CrossRef]
32. Motta, S.E.; Belloni, T.M.; Stella, L.; Muñoz-Darias, T.; Fender, R. Precise mass and spin measurements for a stellar-mass black hole through X-ray timing: The case of GRO J1655-40. *Mon. Not. R. Astron. Soc.* **2014**, *437*, 2554–2565. [CrossRef]
33. Stuchlík, Z.; Kološ, M. Controversy of the GRO J1655-40 Black Hole Mass and Spin Estimates and Its Possible Solutions. *Astrophys. J.* **2016**, *825*, 13. [CrossRef]
34. Hurley, D.J.; Callanan, P.J.; Elebert, P.; Reynolds, M.T. The mass of the black hole in GRS 1915+105: New constraints from infrared spectroscopy. *Mon. Not. R. Astron. Soc.* **2013**, *430*, 1832–1838. [CrossRef]
35. Kato, S. Mass and Spin of GRS 1915+105 Based on a Resonance Model of QPOs. *Publ. Astron. Soc. Jpn.* **2004**, *56*, L25–L28. [CrossRef]